Wind Tunnel Wall Corrections for Two-Dimensional Testing up to Large Angles of Attack

Timmer, W. A.

DOI
10.1007/978-3-030-31307-4_27

Publication date
2022

Document Version
Final published version

Published in
Handbook of Wind Energy Aerodynamics

Citation (APA)
Timmer, W. A. (2022). Wind Tunnel Wall Corrections for Two-Dimensional Testing up to Large Angles of Attack. In *Handbook of Wind Energy Aerodynamics: With 678 Figures and 33 Tables* (pp. 601-629). Springer. https://doi.org/10.1007/978-3-030-31307-4_27

Wind Tunnel Wall Corrections for Two-Dimensional Testing up to Large Angles of Attack

17

W. A. Timmer

Contents

Introduction . . . 602
Blockage in Attached Flow . . . 603
General Form . . . 603
Solid and Wake Blockage . . . 605
Wake Buoyancy . . . 609
Lift Interference . . . 610
Overview of Corrections on Coefficients for Streamlined Flow . . . 611
Correction of the Pressure Distribution . . . 612
Correction of Measurements in the Deep-Stall Region . . . 615
Maskell's Method . . . 616
Corrections on Drag . . . 616
The Wall Pressure Signature Method . . . 622
The Source-Source-Sink Method . . . 624
The Matrix Version of the Wall Signature Method . . . 626
Data Accuracy . . . 627
Summary . . . 628
References . . . 628

Abstract

An accurate representation of two-dimensional airfoil characteristics measured in a wind tunnel generally requires the inclusion of corrections for interference effects that exist due to the presence of the wind tunnel walls. This chapter discusses the most commonly used correction schemes both for streamlined and separated flow regimes. The classical correction method based on small velocity perturbations gives very good results up to angles of attack of about 20 degrees

W. A. Timmer (✉)
Faculty of Aerospace Engineering, Delft University of Technology, Delft, The Netherlands
e-mail: w.a.timmer@tudelft.nl

B. Stoevesandt et al. (eds.), *Handbook of Wind Energy Aerodynamics*,
https://doi.org/10.1007/978-3-030-31307-4_27

for chord-to-tunnel height ratios c/h up to 0.36. Even with separation of the boundary layer at a chord location of 30% the corrected pressure distribution matches that of a much smaller model with c/h = 0.15. In the deep-stall range of angles of attack, where the flow separates from the leading edge, the method based on the wake analysis by Maskell with a blockage factor of 0.96 seems to give good results for two-dimensional models up to c/h values of 0.27. A comparison with measurements corrected with the matrix version of the pressure signature method, which uses the pressure distribution on the tunnel walls, shows that the latter leads to slightly larger corrections. Maskell's method, for which the blockage parameter of 0.96 apparently is based on a single measurement of a two-dimensional flat plate, seems to give better results when a value of 1.03 is used.

Keywords

Wall corrections · Wake blockage · Solid blockage · Wake buoyancy · Lift interference · Deep stall · Maskell method · Pressure signature method · Source-source-sink method

Introduction

The two-dimensional aerodynamic characteristics of dedicated airfoils play a prominent role in the design of wind turbine blades. As long as the flow is attached and the airfoil surface is smooth, numerical codes are able to predict the airfoil force and moment coefficients to a satisfying degree of accuracy. However, when the angle of attack increases beyond the stall angle and boundary layer separation starts to move forward, or when the leading edge area of the airfoil is contaminated or degraded, or when flow dynamics play a significant role, these predictions increasingly lose their accuracy. At this point, wind tunnel measurements are still indispensable to determine the performance. Due to considerations of energy consumption and flow quality and stability the great majority of wind tunnel tests is performed in closed test sections. When a wind tunnel model is placed inside a closed test section the presence of the wind tunnel walls alters the flow field around the model. The model and its wake partly block the passage leading to a local increase of the velocity and the expanding wake induces a pressure gradient in flow direction referred to as wake buoyancy. In addition, the curvature of the streamlines associated with lift generated by the model will be affected by the straight walls of the tunnel.

With increasing rotor diameter, blade design requires airfoil performance data at higher Reynolds numbers. This leads to existing wind tunnel facilities being used with increasingly larger model chords for two-dimensional testing, giving larger blockages in the same angle-of-attack range. In the following paragraphs examples and the applicability of the most common correction schemes for streamlined flow and for separated flow will be explored, each in their own angle-of-attack range.

Blockage in Attached Flow

Interference effects in wind tunnel testing have been the subject of a large number of publications, starting as early as the late 1920s with the work of Lock (1929) and Glauert (1933). The classical correction equations most commonly used in two-dimensional sub-sonic wind tunnel testing find their origin in the assumption of linearized potential flow between the model and the walls. With a (limited) number of singularities, such as vortices to represent the lift, sources for the wake and source-sink doublets to represent the model volume, a theoretical model of the object and its wake is made. The method of images is then used to calculate the interference effects at the model location. The corrections refer to a situation in which the thickness and camber of the airfoil are small, the chord is small with respect to the tunnel height, and the induced velocities everywhere in the test section are small compared to the undisturbed flow velocity. This justifies the neglect of higher powers and products of the interference factors and enables the superposition of interference effects and consequently makes it possible to consider the influence of camber and thickness and of model and wake blockage separately.

General Form

In a closed test section the presence of the model and its wake gives rise to an increase at the model location of the undisturbed (apparent) velocity U′:

$$U = (1 + \varepsilon_b)U' \tag{1}$$

where ϵ_b is the total blockage factor. The prime denotes the uncorrected value.

In its simplest form an arbitrary nondimensional force coefficient C_a in an incompressible flow can be corrected for blockage according to

$$C_a = \frac{C'_a}{(1 + \varepsilon_b)^2} \tag{2}$$

For small blockage factors (2) may be written as

$$C_a = C'_a(1 - 2\varepsilon_b) \tag{3}$$

However, when the effect of compressibility in the correction is included, the equations take a slightly different form. The corrected-uncorrected dynamic pressure ratio is written as:

$$\frac{q}{q'} = \frac{\rho}{\rho'}\left(\frac{U}{U'}\right)^2 \tag{4}$$

The true density at the model is related to the apparent density $\rho\prime$ by the isentropic relation

$$\frac{\rho}{\rho'} = \left\{1 - \frac{\gamma - 1}{2} M'^2 \left[\left(\frac{U}{U'}\right)^2 - 1\right]\right\}^{\frac{1}{\gamma-1}} \tag{5}$$

where M′ is the uncorrected Mach number. With equation 1 and the ratio of specific heats for air $\gamma = 1.4$ we find:

$$\frac{\rho}{\rho'} = \left\{1 - 0.2M'^2 \left[(1 + \varepsilon_b)^2 - 1\right]\right\}^{2.5} \tag{6}$$

Now the combination of equations (1), (4), and (6) is sufficient to correct an arbitrary force coefficient c_a for blockage including the effect of compressibility using

$$c_a = c'_a \left(\frac{q'}{q}\right) \tag{7}$$

Equation (6) can be further simplified by application of the binomial theorem

$$(a + b)^n = a^n + na^{(n-1)}b + \frac{n(n-1)}{2!}a^{n-2}b^2 \ldots\ldots\ldots\ldots \tag{8}$$

Neglect of higher powers of ε_b then gives

$$\frac{\rho}{\rho'} = 1 - M'^2\varepsilon_b \tag{9}$$

Combining (1), (4), and (9) we find

$$\frac{q}{q'} = \left(1 - M'^2\varepsilon_b\right)(1 + \varepsilon_b)^2 \tag{10}$$

and written to the first order of ϵ_b we arrive at

$$\frac{q}{q'} = \left(1 + (2 - M'^2)\varepsilon_b\right) \tag{11}$$

The effect of neglecting higher order terms of the blockage factor on the lift and drag coefficients for moderate angles of attack and reasonably sized models stays well below 0.5%.

In the same manner the impact of blockage on the Reynolds number can be found using

$$Re = Re' \left(\frac{\rho}{\rho'}\right)\left(\frac{\mu'}{\mu}\right)\left(\frac{U}{U'}\right) \tag{12}$$

According to von Kármán and Tsien (Allen and Vincenti 1947) the ratio of the coefficients of viscosity is related to the ratio of temperatures by

$$\left(\frac{\mu}{\mu'}\right) = \left(\frac{T}{T'}\right)^{0.76} \tag{13}$$

The isentropic relation for the temperature is

$$\frac{T}{T'} = \left\{1 - \frac{\gamma - 1}{2} M'^2 \left[\left(\frac{U}{U'}\right)^2 - 1\right]\right\} \tag{14}$$

To the first order this leads to

$$Re = Re' \left(1 + (1 - 0.7M'^2)\varepsilon_b\right) \tag{15}$$

Likewise the correction of the Mach number is determined, writing

$$M = M' \left(\frac{U}{U'}\right)\left(\frac{a'}{a}\right) \tag{16}$$

where a′ is the uncorrected speed of sound. In an ideal gas the speed of sound is only proportional to the square root of the temperature, which gives

$$M = M' \left(\frac{U}{U'}\right)\sqrt{\frac{T'}{T}} \tag{17}$$

Written to the first order, this leads to

$$M = M' \left(1 + (1 + 0.2M'^2)\varepsilon_b\right) \tag{18}$$

Solid and Wake Blockage

If it is assumed that the model is small compared to the tunnel test section and that the lift is not too large, the blockage due to the model (solid blockage) and that due to the wake (wake blockage) can be treated separately:

$$\varepsilon_b = \varepsilon_s + \varepsilon_w \tag{19}$$

Solid Blockage

Solid blockage is the result of the displacement of streamlines in the tunnel due to the volume of a non-lifting model. In an analysis by Lock the base profile in the center of the tunnel at zero incidence is modeled by a single doublet. The effect

of the walls in two dimensions is replaced by an infinite system of doublet images extending on both sides of the model spaced at a distance equal to the test section height. By symmetry the velocity component normal to the walls is zero.

The net effect of the tunnel walls upon the flow at the base profile is an increase in effective axial velocity of magnitude

$$\varepsilon_s = \frac{\pi^2}{12}\left(\frac{c}{h}\right)^2\left(\frac{t}{c}\right)^2\frac{1}{\beta^3}\lambda_2 \tag{20}$$

where λ_2 is a parameter related to the airfoil thickness t, and the airfoil surface pressure distribution. β is the Prandtl-Glauert compressibility correction factor $\sqrt{1-M'^2}$, c is the airfoil chord, and h is the effective tunnel height. An approximation for λ_2 was given bij Glauert, $\lambda_2 = 2A/(\pi t^2)$, which effectively turns Eq. 20 into

$$\varepsilon_s = \frac{\pi}{6}\frac{A}{\beta^3 h^2} \tag{21}$$

where A is the cross-section area of the airfoil. Thompson (Garner et al. 1966) suggests a relation in which the thickness of the airfoil is more prominently accounted for:

$$\varepsilon_s = \frac{\pi}{6}\left[1 + 1.2\beta\left(\frac{t}{c}\right)\right]\frac{A}{\beta^3 h^2} \tag{22}$$

The airfoil cross-section area A can be written as a combination of a factor and the product of maximum thickness and chord. For airfoil families resulting from analytical descriptions of the shape this factor is often a constant. For the old 4-digit NACA series of airfoils based on the 00xx thickness form, for example, A= 0.69∗t∗c. The cross-section area of the 6-digit NACA 63-series, though strictly speaking not the result of a prescribed shape but rather of a systematically prescribed pressure distribution, can be approximated using a factor of 0.62.

Allen and Vincenti found a similar equation as (20) but they use the expression

$$\Lambda = 4\left(\frac{t}{c}\right)^2\lambda_2 \tag{23}$$

They write:

$$\varepsilon_s = \frac{\Lambda\sigma}{\beta^3} \tag{24}$$

with the tunnel blockage factor

$$\sigma = \frac{\pi^2}{48}\left(\frac{c}{h}\right)^2 \tag{25}$$

The body-shape factor Λ is defined as

$$\Lambda = \frac{16}{\pi}\int_0^1 \frac{y}{c}\sqrt{(1-C_p)\left(1+\left(\frac{dy}{dx}\right)^2\right)}d\frac{x}{c} \tag{26}$$

in which C_p is the inviscid zero-incidence pressure coefficient at the chord-wise station x and y is the ordinate of the symmetric (base) profile. Allen and Vincenti give values for a number of base profiles.

With relation (26) the shape factor for the NACA 63-0xx series of airfoils has been calculated using the inviscid pressure coefficients at 300 chord stations. The present Λ-values for the NACA 63 series in the thickness range of interest to wind turbine blades are represented by equation 27:

$$\Lambda_{NACA63} = 1.4890\left(\frac{t}{c}\right)^2 + 1.6143\left(\frac{t}{c}\right) + 0.0023 \tag{27}$$

The parameter t/c is the maximum relative thickness of the airfoil in fractions of the chord. Figure 1 gives a comparison with the values presented by Allen and Vincenti. Their lower values can be attributed to the much lower number of pressure stations taken for the integration.

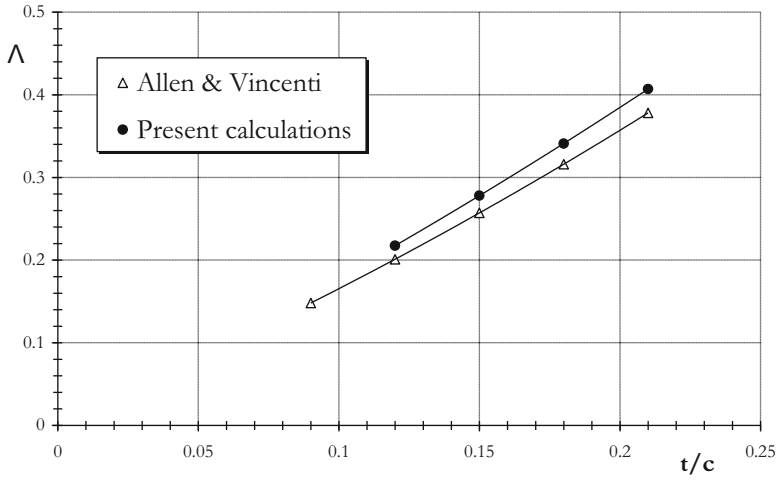

Fig. 1 The body shape factor Λ for the Naca 63 series of airfoils

Equations (22) and (24) do not differ very much in their calculation of the solid blockage factor. For an 18% thick laminar airfoil like NACA 63_3-418 and a typical Mach number of 0.2 the factor by Allen and Vincenti is 1% lower. When using a 30% thick airfoil such as DU 97-W-300 the difference increases to -1.6%. The differences go up with decreasing Mach number and are around zero close to M = 0.4.

The solid blockage equations were essentially derived with the assumption that the blockage is independent of lift. Based on the work of Batchelor (Garner et al. 1966), it is suggested that the simple theory expressed in equations (22) or (24) can be adapted to deal with the solid blockage of an airfoil at an angle of attack α by writing:

$$\varepsilon_s(\alpha) = \varepsilon_s \left[1 + \beta \frac{1.1}{(t/c)} \alpha^2 \right] \tag{28}$$

with α expressed in radians.

Wake Blockage

The wake effect is simulated by a system of source images. Source strength is related to the measured drag coefficient using conservation laws with the boundary condition that the flow field far upstream remains unchanged. Under these assumptions the wake blockage at the tunnel center can be determined (Garner et al. 1966) from:

$$\varepsilon_w = \frac{1}{4} \left(\frac{c}{h} \right) \frac{1 + 0.4M'^2}{\beta^2} C'_d \tag{29}$$

The Total Blockage Factor

The total blockage factor can now be composed from the contributions of the solid and the wake blockages. Using the notation of Allen and Vincenti this gives:

$$\varepsilon_b = \frac{\Lambda \sigma}{\beta^3} \left[1 + 1.1\beta \frac{\alpha^2}{(t/c)} \right] + \frac{1}{4} \left(\frac{c}{h} \right) \frac{1 + 0.4M'^2}{\beta^2} C'_d \tag{30}$$

The two-dimensional approach of the derivations essentially implies a rectangular test section. However, many wind tunnels have working sections with corner fillets, which raises the question what value of the tunnel height h should be used. From considerations of continuity an effective height h_e can be derived from the test section area divided by the span of the model.

Insertion of Eq. (30) into Eq. (10) or (11) yields the change of the dynamic pressure due to the blockage inside the test section, which can be used with Eq. (7) to correct the force and moment coefficients for blockage. For small values of the blockage factor we may use

$$\frac{q'}{q} = \frac{1}{\left(1 + (2 - M'^2)\varepsilon_b\right)} \approx \left(1 - (2 - M'^2)\varepsilon_b\right) \tag{31}$$

To correct forces and moments for blockage using Eq. 31 we may write

$$C_a = C'_a \frac{q'}{q} = C'_a \left(1 - (2 - M'^2)\varepsilon_b\right) \tag{32}$$

Note that for incompressible flow ($M' = 0$) this equation equals (3).

Wake Buoyancy

Apart from a blockage effect, the developing wake induces a velocity increase in flow direction and consequently, applying Bernoulli's equation, also gives rise to a pressure gradient along the model which would not exist in free air. This pressure gradient is felt by the model as buoyancy and the associated increase in drag follows from a derivation by Allen and Vincenti based on the work of Glauert:

$$\Delta D = D' \left(\frac{1 + 0.4M'^2}{\beta^3} \Lambda\sigma\right) \tag{33}$$

The true drag in free air is given by

$$D = D' - \Delta D = D' \left(1 - \frac{1 + 0.4M'^2}{\beta^3} \Lambda\sigma\right) \tag{34}$$

With the definition of the drag coefficients we find

$$D = c_d q c = c'_d q' c \left(1 - \frac{1 + 0.4M'^2}{\beta^3} \Lambda\sigma\right) \tag{35}$$

The drag coefficient in free air, with reference to the true dynamic pressure follows from

$$c_d = c'_d \left(1 - \frac{1 + 0.4M'^2}{\beta^3} \Lambda\sigma\right) \frac{q'}{q} \tag{36}$$

Combined with Eq. (31) and written to the first order the corrected drag coefficient is given by

$$c_d = c'_d \left[1 - \frac{1 + 0.4M'^2}{\beta^3} \Lambda\sigma - \left(2 - M'^2\right) \varepsilon_b\right] \tag{37}$$

with ε_b given by Eq. (30).

There is some debate about the applicability of the buoyancy correction if the drag is derived from the pressures in the wake, reduced in the usual way. Allen and Vincenti state that the correction equations are primarily derived for drag measured with a balance, but that for normal chord-to-height ratio's values differ by less than 0.5%. Rogers (Garner et al. 1966) argues that in particular the wake buoyancy equation should not be applied when the drag is measured with a wake rake. It is indeed questionable whether the impact of the drag increase due to the wake-wall interference is captured by the wake rake data reduction, since the speed-up due to the expanding wake for reasons of continuity mainly takes place outside the wake, which is discarded if the wake survey method is used in the conventional way. It can be argued that the wake buoyancy correction should only be applied if the drag is derived from balance measurements or from the model pressure distribution.

Lift Interference

A straight walled closed test section prevents the normal curvature of the flow around an airfoil producing lift since the streamlines along the walls are straight. As a result the model appears to have more camber showing increased lift and moment coefficients and an induced upwash, changing the angle of attack.

This problem of lift interference (streamline curvature) is evaluated o.a. by Allen and Vincenti for a thin airfoil with its chord on the tunnel center line. They approximate the load on the airfoil by distributed vorticity along the chord. Vortex theory is used on a system of images with alternating signs to mimic the tunnel walls.

With the requirement that the distribution of lift along the chord and especially the magnitude of the lift component near the leading edge of the airfoil shall be the same both in free air and in the tunnel, their evaluation leads to a set of relations in the form of

$$\alpha = \alpha' + \Delta\alpha$$

$$c_l = \left(c_l' + \Delta c_l\right)\frac{q'}{q} \tag{38}$$

$$c_m = \left(c_m' + \Delta c_m\right)\frac{q'}{q}$$

where the increments quantify the effect of the lift interference to the order $(c/h)^2$ and are defined as

$$\Delta\alpha = \frac{\sigma}{2\pi\beta}\left(C_l' + 4C_m'\right)$$

$$\Delta C_l = -C_l'\frac{\sigma}{\beta^2} \tag{39}$$

$$\Delta C_m = C_l' \frac{\sigma}{4\beta^2}$$

and q'/q can be derived from Eq. (11). The angle of attack is in radians. According to Garner et al. (1966) the applicability of these relations is restricted to $c<0.4\beta h$. Based on the work of Havelock (Garner et al. 1966) the equations of (39) are expanded to the order $(c/h)^4$

$$\Delta\alpha = \frac{\sigma}{2\pi\beta}\left(C_l' + 4C_m'\right) - 0.525\frac{\sigma^2}{\pi\beta^3}C_l' \tag{40}$$

$$\Delta C_l = C_l'\left(-\frac{\sigma}{\beta^2} + 5.25\frac{\sigma^2}{\beta^4}\right) \tag{41}$$

$$\Delta C_m = C_l'\left(\frac{\sigma}{4\beta^2} - 1.05\frac{\sigma^2}{\beta^4}\right) \tag{42}$$

Overview of Corrections on Coefficients for Streamlined Flow

A combination of the correction relations in the foregoing chapters for lift interference, blockage, and wake buoyancy leads to the following set of correction equations

$$\alpha = \alpha' + \frac{\sigma}{2\pi\beta}\left(C_l' + 4C_m'\right) \tag{43}$$

$$C_l = C_l'\left[1 - \frac{\sigma}{\beta^2} + 5.25\frac{\sigma^2}{\beta^4} - \frac{(2-M'^2)}{\beta^3}\Lambda\sigma\left(1 + \frac{1.1\beta}{(t/c)}\alpha^2\right) - \frac{(2-M'^2)(1+0.4M'^2)}{4\beta^2}\left(\frac{c}{h}\right)C_d'\right] \tag{44}$$

$$C_d = C_d'\left[1 - \Delta C_d^* - \frac{(2-M'^2)}{\beta^3}\Lambda\sigma\left(1 + \frac{1.1\beta}{(t/c)}\alpha^2\right) - \frac{(2-M'^2)(1+0.4M'^2)}{4\beta^2}\left(\frac{c}{h}\right)C_d'\right] \tag{45}$$

The wake buoyancy correction $\Delta C_d^* = 0$ for wake rake measurements and $\Delta C_d^* = \Lambda\sigma\frac{1+0.4M'^2}{\beta^2}$ for drag measured with a balance or calculated from the pressure distribution.

$$C_m = C'_m\left[1 - \frac{(2-M'^2)}{\beta^3}\Lambda\sigma\left(1+\frac{1.1\beta}{(t/c)}\alpha^2\right) - \frac{(2-M'^2)(1+0.4M'^2)}{4\beta^2}(\frac{c}{h})C'_d\right] + \\ + C'_l(\frac{\sigma}{4\beta^2} - 1.05\frac{\sigma^2}{\beta^4}) \tag{46}$$

$$q = q'\left[1 + \frac{(2-M'^2)}{\beta^3}\Lambda\sigma\left(1+\frac{1.1\beta}{(t/c)}\alpha^2\right) + \frac{(2-M'^2)(1+0.4M'^2)}{4\beta^2}(\frac{c}{h})C'_d\right] \tag{47}$$

$$Re = Re'\left[1 + \frac{(1-0.7M'^2)}{\beta^3}\Lambda\sigma\left(1+\frac{1.1\beta}{(t/c)}\alpha^2\right) \\ + \frac{(1-0.7M'^2)(1+0.4M'^2)}{4\beta^2}(\frac{c}{h})C'_d\right] \tag{48}$$

The angle of attack in the equations is expressed in radians. In equation (43) the term dealing with $(c/h)^4$ is omitted because it is negligibly small. For the angle of attack expressed in degrees we write:

$$\alpha = \alpha' + \frac{57.3\sigma}{2\pi\beta}\left(C'_l + 4C'_m\right) \tag{49}$$

Correction of the Pressure Distribution

The solid and wake blockage and the lift interference correction should obviously also appear in the correction of the pressure distribution. The most straightforward equations often used are:

$$Cp_u = (C'_{p_u} + \Delta C_p)\frac{q'}{q} \tag{50}$$

$$Cp_l = (C'_{p_l} - \Delta C_p)\frac{q'}{q} \tag{51}$$

in which the indices u and l denote the upper and lower surface, respectively. The ratio of the uncorrected and corrected dynamic pressures is given by equation (31). The correction for lift interference ΔC_p follows from

$$\Delta Cp = \frac{4}{\pi}\left(\frac{\sigma^2}{\beta^2} - \frac{5.25}{\beta^4}\sigma^4\right)C'_l\sqrt{\frac{x}{c}\left(1-\frac{x}{c}\right)} \tag{52}$$

given to the 4th power of c/h.

Allen and Vincenti argue that the two contributions should be treated separately; a correction for the blockage due to the base profile and a correction for streamline curvature applied to the lift per unit chord. To this end the pressure distribution of an airfoil is expressed as

$$Cp_u = 1 - \frac{\left[\left(1 - C_{p_{sym}}\right) + \frac{1}{4}\left(C_{p_l} - C_{p_u}\right)\right]^2}{\left(1 - C_{p_{sym}}\right)} \tag{53}$$

$$Cp_l = 1 - \frac{\left[\left(1 - C_{p_{sym}}\right) - \frac{1}{4}\left(C_{p_l} - C_{p_u}\right)\right]^2}{\left(1 - C_{p_{sym}}\right)} \tag{54}$$

where $C_{p,sym}$ is the pressure coefficient of the base (symmetrical) profile.

For the blockage correction as a result of the presence of the base profile the lift is removed by taking the average of the kinetic pressures on the upper and lower surface at the same chord location. If the pressure orifices on upper and lower surface do not have the same chord location (x-ordinate), an interpolation between two pressure orifices is performed. If the pressure coefficients on upper and lower surface are related to the true instead of the apparent dynamic pressure we can write:

$$Cp_u = 1 - \frac{\left[\left(\frac{\sqrt{q_u^*}+\sqrt{q_l^*}}{2}\right)^2 + \left(\frac{q_u^*+q_l^*}{4} - \left(\frac{\sigma}{\pi\beta^2} - 5.25\frac{\sigma^2}{\pi\beta^4}\right)C_l'\sqrt{1-\left(1-\frac{2x}{c}\right)^2}\right)\right]^2}{\left(\frac{\sqrt{q_u^*}+\sqrt{q_l^*}}{2}\right)^2} \tag{55}$$

$$Cp_l = 1 - \frac{\left[\left(\frac{\sqrt{q_u^*}+\sqrt{q_l^*}}{2}\right)^2 - \left(\frac{q_u^*+q_l^*}{4} - \left(\frac{\sigma}{\pi\beta^2} - 5.25\frac{\sigma^2}{\pi\beta^4}\right)C_l'\sqrt{1-\left(1-\frac{2x}{c}\right)^2}\right)\right]^2}{\left(\frac{\sqrt{q_u^*}+\sqrt{q_l^*}}{2}\right)^2} \tag{56}$$

where q_u^* and q_l^* are given by:

$$q_u^* = \left(1 - Cp_u'\right)\frac{q'}{q} \tag{57}$$

respectively

$$q_l^* = \left(1 - Cp_l'\right)\frac{q'}{q} \tag{58}$$

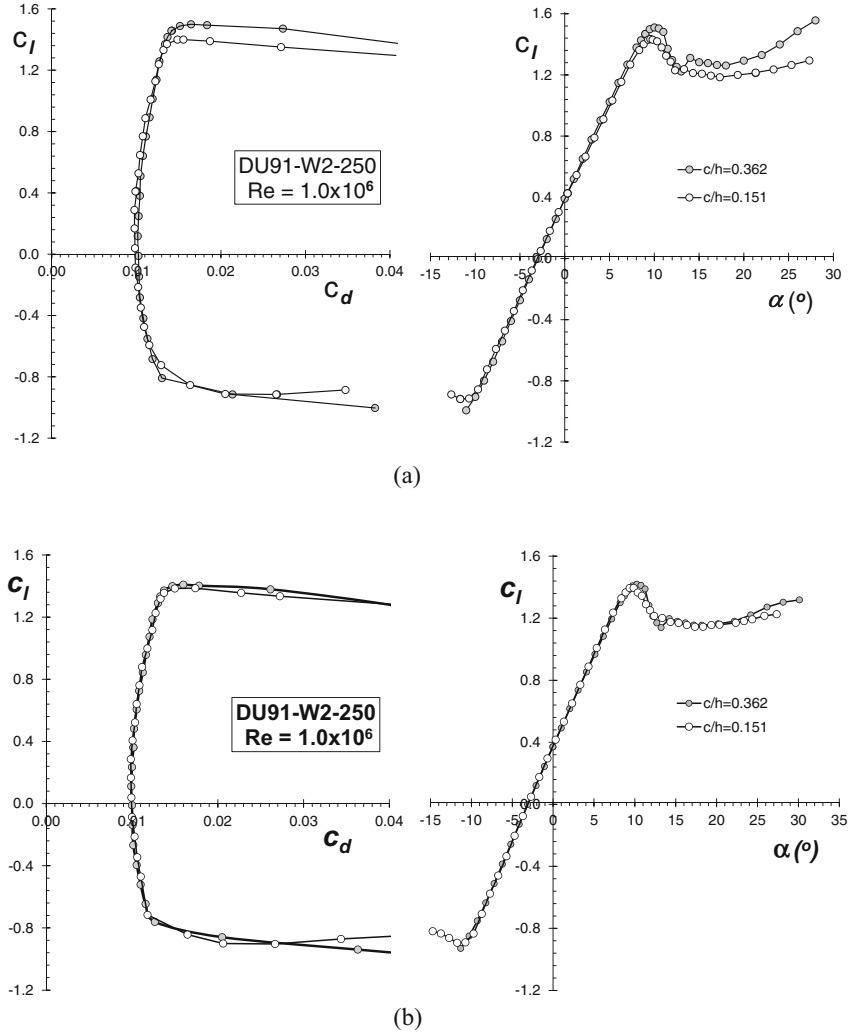

Fig. 2 The uncorrected (**a**) and corrected (**b**) characteristics of airfoil DU91-W2-250 for two different chord-to-height ratios. Data corrected for Mach number

The ratio of the corrected and uncorrected dynamic pressures in the latter equations can be calculated from (31).

The pressure distribution corrected in this way corresponds to the corrected angle of attack and lift- and moment coefficients

Figure 2 presents the measured two-dimensional characteristics of the 25% thick airfoil DU91-W2-250 for two different models with chords of 0.25 m and 0.60 m. The tests were performed in the 1.25x1.80 m Delft University (TUDelft) Low-speed

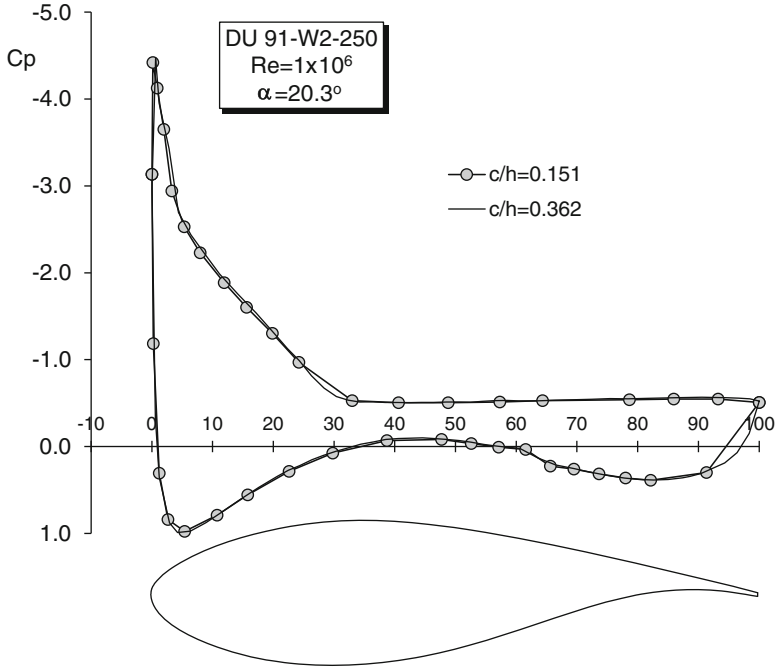

Fig. 3 The corrected pressure distributions for two values of the chord-height ratio at an angle of attack of 20.3 degrees

Low-turbulence wind tunnel (LTT). The test section has 0.42 m wide corner fillets and the models were set up vertically, which, leads to an effective height of 1.656 m, giving c/h values for the two different models of 0.151 and 0.362. The graph shows a very good match between the corrected characteristics, both for the lift and the drag curves. Noteworthy is the fact that even up to an angle of attack of 20 degrees the correction scheme is capable of matching the lift curves. Figure 3 shows the pressure distributions for both models at $\alpha = 20.3^{\circ}$. Even with flow separation at about 30% of the chord the corrected base pressures match very well.

Correction of Measurements in the Deep-Stall Region

With increasing separation on the wind tunnel model the blockage due to the wake becomes increasingly important and eventually will become a dominant factor of the total blockage inside the test section. In these cases the classical treatment of small perturbations due to blockage is no longer valid. In the deep-stall region of angles of attack, where the flow separates from the leading edge, the two-dimensional airfoil model starts to behave like a bluff body.

Correction methods accounting for the wall interference of bluff bodies in closed test sections can be divided into methods using the measured drag of the model and those relying on the measured pressure distribution on the walls: the wall-signature method.

Maskell's Method

Maskell (1963) developed a method to correct for wall interference effects when dealing with separated flow over bluff bodies. In its simplest form the method only uses the measured drag due to separation and some geometric parameters to establish a dynamic pressure correction. His method was primarily developed for the flow over bluff bodies, but can also be used for stalled wings since the flow in the heavily separated region of the model shows resemblance with bluff body wakes.

Corrections on Drag

Maskell considers the flow depicted in Fig. 4. The wake of the bluff body is represented by a stream surface originating from the edge of the body, extending downstream. In plane 2 the cross section of the wake reaches its maximum. Plane 1 is far ahead of plane 2 and contains the undisturbed velocity U. A constant pressure p_b is present on the surface of this wake bubble with associated velocity kU, where k is the ratio of wake edge velocity over undisturbed velocity. This pressure is equal to the base pressure acting at the back of the bluff body. Maskell argues that the pressure distribution on the model in the test section is invariant under the constraint imposed by the walls. This means that the flow field simply scales with the amount of blockage, which leads to the expression:

$$\frac{C'_D}{k'^2} = \frac{C'_D}{(1 - C'_{p_b})} = const. \tag{59}$$

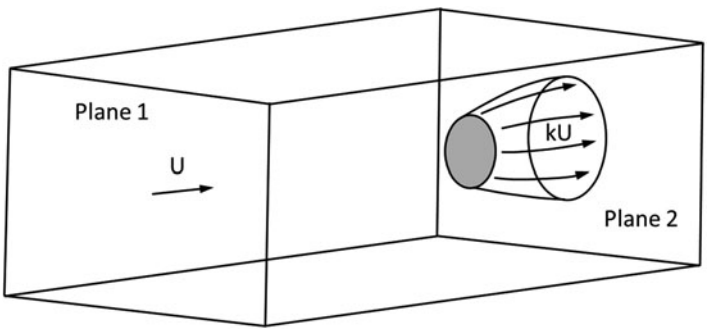

Fig. 4 The bluff body flow model considered by Maskell (1963)

where C'_D is the measured drag coefficient, defined as $D'/q'S$, with S a representative area of the body and q' the dynamic pressure, and C'_{pb} is the base pressure coefficient. Maskell confirmed experimentally the invariance principle using drag and base pressure measurements on a set of square flat plates positioned normal to the flow in two different wind tunnels, thus varying the amount of blockage. The S/C values, where C is the cross-sectional area of the tunnel and S the frontal area of the plates, ranged from 0.0019 to 0.0451 and base pressure coefficients from −0.386 to −0.589. Also for two-dimensional flow this invariance can be shown, as is presented in Fig. 5, with measurements on two DU91-W2-250 airfoil models in the TUDelft LTT, giving relatively small values of S/C, but well outside the range tested by Maskell (0.091 and 0.151, respectively).

Considerations of conservation of momentum in the fluid passing the control surface shown in Fig. 4 leads to the expression

$$C'_D = m\left(k'^2 - 1 - m\frac{S}{C}\right) \tag{60}$$

where m= B/S and B is the maximum cross section of the wake. Equation (60) was derived with the assumption that the contribution to the momentum balance of the in-plane orthogonal components of the velocity in cross-section 1, far ahead of the object, and in cross-section 2 outside the wake are negligibly small. This is true for two-dimensional flow; however, with the argument that there is a tendency of the

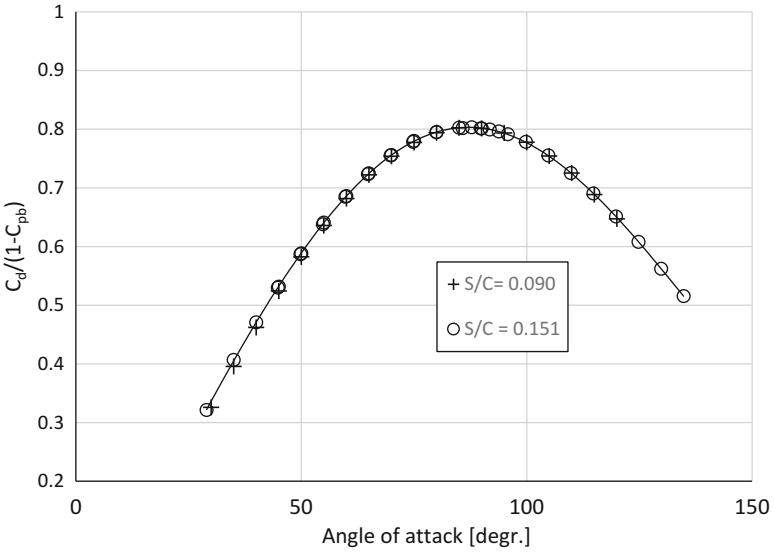

Fig. 5 The invariance of C_D/k^2 (eq. 59) for two different blockage factors of airfoil DU91-W2-250, Re = 0.7×10^6

wakes of three-dimensional bodies to become axial-symmetric far downstream this also holds for other objects.

If the increase of the velocity in the closed test section would only come from blockage due to the presence of the wake, Maskell arrives at

$$\frac{k'^2}{k^2} = \frac{C'_D}{C_{D_M}} = 1 + \frac{C_{D_M}}{k^2 - 1}\frac{S}{C} \tag{61}$$

where C_{D_M} is the corrected drag coefficient. However, wall constraint impacts the free expansion of the wake. The effect of this wake distortion on the value of B in Eq. (60) was determined by the assumption that this distortion is proportional to the contraction of the stream outside the wake (C-B)/C. Neglecting terms in the order of $(S/C)^2$ Maskell found that the net result of incorporating wake distortion in the derivation is to replace the corrected drag coefficient in Eq. (61) by the measured drag coefficient:

$$\frac{C'_D}{C_{D_M}} = 1 + \frac{C'_D}{k^2 - 1}\frac{S}{C} \tag{62}$$

Hence

$$C_{D_M} = \frac{C'_D}{1 + \theta \frac{S}{C} C'_D} \tag{63}$$

where θ is the blockage factor for bluff-body flow:

$$\theta = \frac{1}{k^2 - 1} \tag{64}$$

The parameter k^2 can be derived from Eq. 44 through iteration using the measured mean base pressure as a starting value, $(k^2)_0 = k'^2$:

$$(k^2)_n = k'^2 \left[1 + \frac{1}{(k^2)_{n-1} - 1} C'_D \frac{S}{C}\right]^{-1} \tag{65}$$

Two-Dimensional Models

To calculate the blockage factor for a two-dimensional flat plate Maskell used experimental results from Fage and Johansen (1927), who presented measurements on a number of two-dimensional flat plates with different chords. For one of the plates also the base pressure ($C_p = -1.30$) and the mean pressure along the edge of the wake ($C_p = -1.38$) at 90 degrees angle-of-attack were determined. As indicated, it appeared that these two pressures are not equal, hence the average was used in the calculation. With $C_D = 2.13$ and $S/C = 0.0715$, Eqs. (64) and (65) give $\theta = 0.960$. The corrected drag coefficient is 1.858.

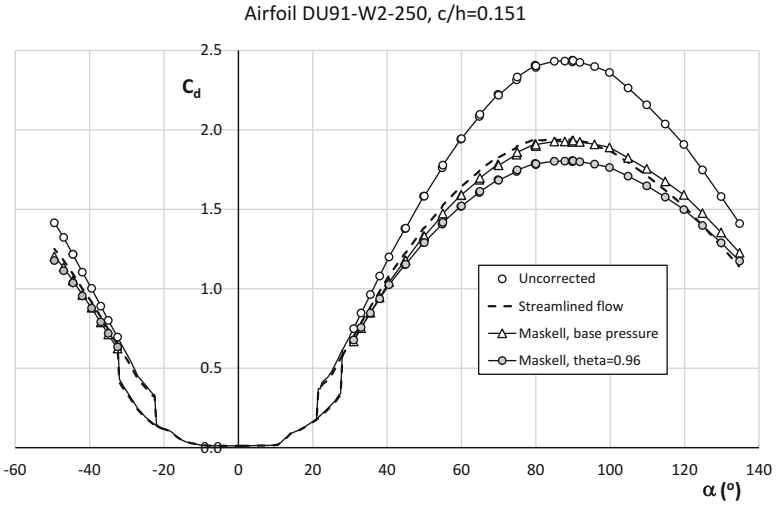

Fig. 6 Comparison of corrected drag curves using various correction schemes. Re $= 0.7 \times 10^6$

The average corrected drag coefficient at 90 degrees incidence of the 4 thin two-dimensional plates tested by Fage and Johansen was 1.86, which deviates appreciably from the at present commonly adopted value between 1.98 and 2.0. This might find its origin in the setup of these tests. The drag was determined from the pressure distribution around the mid-span of the plate with pressure orifices in only one side of the plate. To complete the pressure distribution around the plate, it had to be rotated 180°. For stiffness purposes one side of the plate was not completely flat but formed a wedge with a 3% thickness at mid-chord.

Figure 6 shows the difference in the two-dimensional drag curves corrected with the various methods. Data come from measurements on a 0.25 m chord model in the Delft University LTT, with an S/C (= c/h, with h the effective test section height) value of 0.151. It appears that the method using the base pressures gives results close to those resulting from the correction scheme for streamlined flow. The difference with the curve using Maskell's value of 0.96 for the blockage factor θ is substantial.

The comparison with a 40% smaller model in the same tunnel, depicted in Fig. 7, shows that only the method using $\theta = 0.96$ brings the two drag curves close together, with a difference in the maximum drag coefficient in the order of only 1%.

The conclusion must be that the method based on the model rear pressure does not work for two-dimensional flow with S/C values appreciably larger than those in Maskell's measurements. Despite the fact that the value of 0.96 apparently was derived from one measurement on a two-dimensional flat plate it holds also quite well for airfoil measurements in the deep-stall region.

On basis of the measurements presented in Fig. 7 a value slightly larger than 0.96 for the blockage factor, say in the order of 1 to 1.03, is necessary to match both drag curves. The lower boundary of 1.0 is exactly the value that results from a calculation

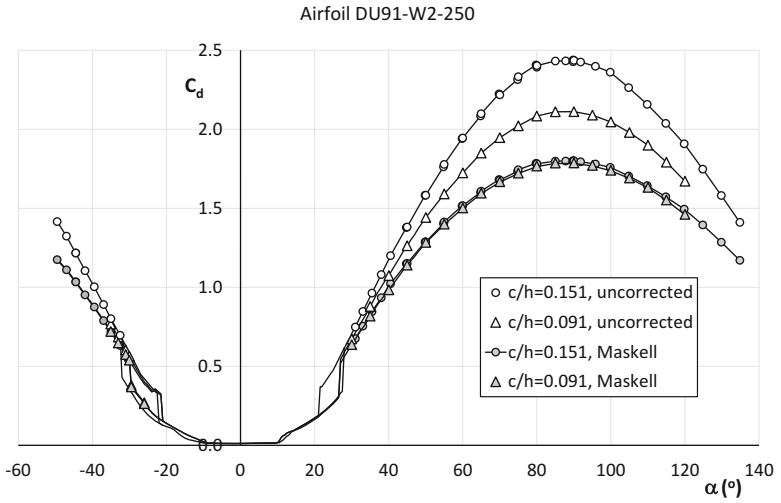

Fig. 7 The corrected drag curves for measurements on two models with c/h values of 0.091 and 0.151 using Maskell's method with $\theta = 0.96$. Re $= 0.7 \times 10^6$

of θ using a base pressure of $C_{pb} = -1.30$ in the test of the flat plate by Fage and Johansen described earlier.

It must be noted that the drag curves shown in Figs. 6 and 7 come from pressure measurements. Depending on the number and distribution of the pressure orifices, especially in the lower surface trailing edge region, the calculated drag coefficient may differ slightly from the one resulting from balance measurements. Hence, when comparing drag curves with different c/h, some of the variations may be attributed to differences in measurement technique.

Strictly, the uncorrected drag coefficient in the blockage parameter $C'_D S/C$ in equation 45 is the one due to separation. For angles in the deep-stall region the full uncorrected value can be used, as the difference is negligibly small.

Correction on the Angle of Attack

When the airfoil is producing lift, the corrections on angle of attack for streamlined flow are based on the fact that the curvature of the streamlines is altered by the presence of the walls. For two-dimensional models in deep stall the streamlines at the model location are on average straight and the increase in lift comes predominantly from the fact that the entire upper surface has a time-averaged constant pressure, which decreases with angle of attack. Hence it can be argued that there is no need for an angle of attack correction in deep stall.

Corrections on Lift and Moment Coefficients

Hackett (1996) recognized that the wake distortion correction in Maskell's method comes as part of a dynamic pressure correction, while it in fact is a drag increment,

which should be removed from the dynamic pressure correction before correcting the lift and moment coefficients.

In a two-step approach Hackett writes:

$$\Delta C_D = C_{D_M} - C_{D_\infty} \tag{66}$$

where C_{D_M} again is the corrected drag coefficient using Maskell's method and $C_{D\infty}$ is the corrected drag coefficient without distortion. Equations (61) and (64) then give

$$C_{D_\infty} = C_{D_M} - \Delta C_D = \frac{C_{D_M}}{1 + \theta \frac{S}{C}\left(C_{D_M} - \Delta C_D\right)} \tag{67}$$

Combining equations (63), (64), and (67) and solving the quadratic equation in ΔC_D yields:

$$\Delta C_D = C_{D_M} - \frac{-1 + \sqrt{1 + 4\theta \frac{S}{C} C'_D}}{2\theta \frac{S}{C}} \tag{68}$$

The lift, moment, and pressure coefficients can now be corrected for wake blockage using

$$\frac{q'}{q} = \frac{C_{D_\infty}}{C'_D} = \frac{1}{1 + \theta \frac{S}{C}\left(C_{D_M} - \Delta C_D\right)} \tag{69}$$

Note that equation (68) needs to return a negative value of ΔC_d as $C_{D\infty}$ is larger than C_{DM}

A comparison of the lift coefficients from the models of Fig. 7 corrected with the dynamic pressure correction according to Eq. 69 is presented in Fig. 8.

The differences in lift coefficients between the two models in the range of angles between maximum lift and deep stall come from a small irregularity near the upper surface leading edge of the smaller model in the vicinity of the pressure orifices.

With the same dynamic pressure ratio the pressure distribution can be corrected:

$$C_p = 1 - (1 - C'_p)\frac{q'}{q} \tag{70}$$

Higher Values of c/h

The systematic neglect of terms in the order of $(S/C)^2$ in Maskell's derivation may limit the applicability of the method for tests with increasingly higher c/h values. Maskell's method has often been found to over-correct at high area ratio's, according to Cooper in Agardograph 336 (Ewald 1998) Fig. 9 may shed some light on the differences that exist when using Maskell's method with $\theta = 0.96$ to correct measurements with c/h values higher than 0.15. The measurements shown

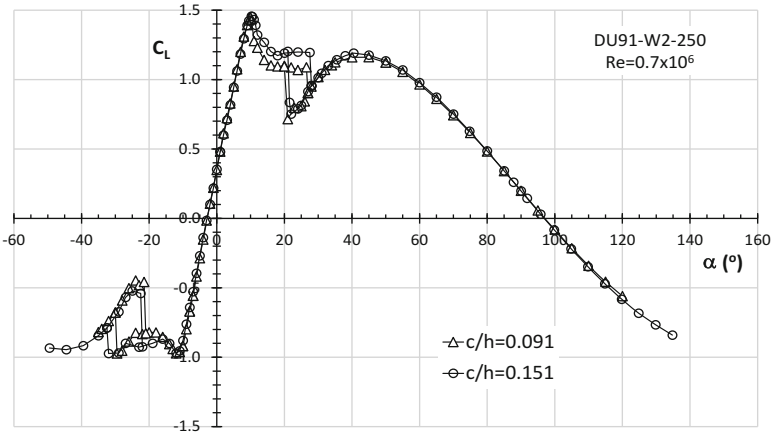

Fig. 8 The aerodynamic characteristics of DU91-W2-250 for two models with c/h=0.091 and 0.151 respectively, corrected with Hackett's two-step version of Maskell's analysis

in Figs. 9 and 10 were performed by Wang et al. (2015) in the NF-3 wind tunnel of Northwestern Polytechnical University in Xi'an, China. Three models of airfoil WA-210 with chord lengths of 0.5, 0.65, and 0.8 meter were tested in the 1.6x3.0 m test section, giving chord-to-height ratios of 0.167, 0.217, and 0.267, respectively. The uncorrected data were taken from the paper and corrected with Maskell's method using $\theta = 0.96$. The Reynolds number was 0.75×10^6 and for clarity of the graph only the high angle of attack region is shown.

It appears that even for the highest c/h value the corrected drag curve does not deviate much from the lowest value, both for positive and negative angles. The differences in the maximum corrected drag coefficient for the lowest and the highest c/h are smaller than 1% and fall well within the experimental error. At these c/h values there seems to be no over correction using Maskell's method to correct the drag.

Figure 10 shows the corresponding lift curves. As is clear from the drag curves, the largest differences occur for angles of attack beyond 90 degrees, which may also have an aerodynamic background, as at these angles for relatively low Reynolds numbers the separation location, and consequently the separation pressure, is very sensitive to changes, for example, additional turbulence, in the inflow.

The Wall Pressure Signature Method

Hackett and Wilsden (1975) presented a method to correct for wall interference effects using the static pressure distribution (signature) on the tunnel walls. Singularities, such as sources and vortices, are distributed along the tunnel centerline producing a theoretical pressure distribution equivalent to the measured distribution.

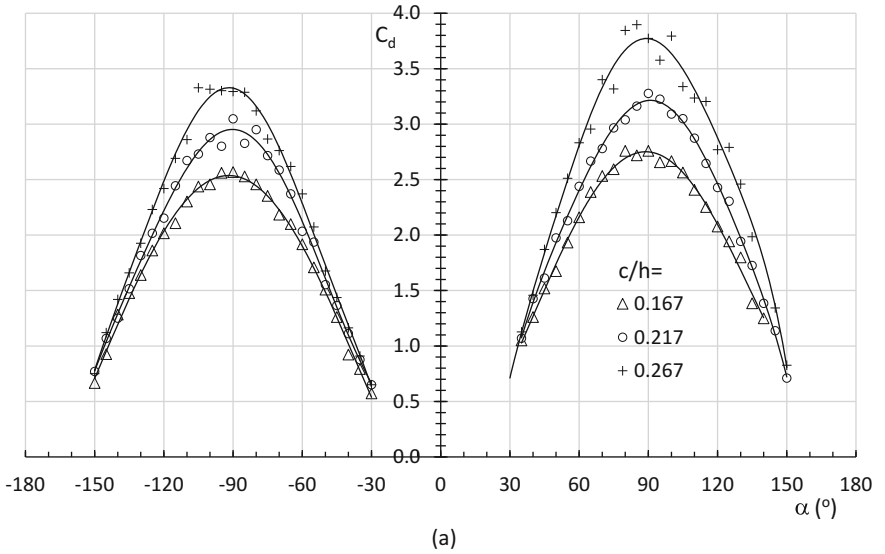

Fig. 9 The uncorrected (**a**) and Maskell-corrected (**b**) drag curves for airfoil WA-210 with varying chord to tunnel height ratio's, Re $= 0.75 \times 10^6$. (Uncorrected data from Wang et al. 2015)

The strength of these singularities is calculated using the perturbation velocity at each pressure location given by

$$\frac{\Delta u(x)}{U} = \sqrt{1 - \Delta C'_p(x)} - 1 \tag{71}$$

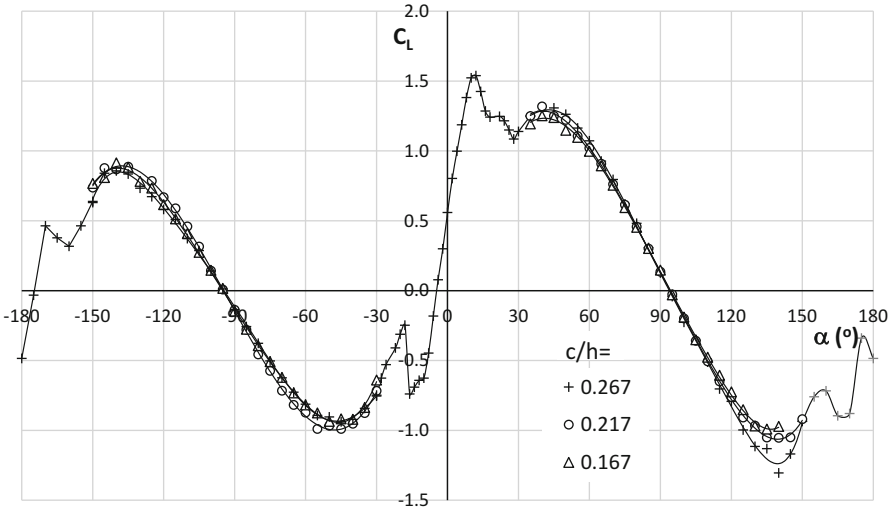

Fig. 10 The corrected lift curves for airfoil WA-210 with varying chord to tunnel height ratio's

where $\Delta C_p'$ is the difference between the pressure distributions with the model installed and with an empty tunnel. Using wall images the interference effects are then determined at the model location.

The Source-Source-Sink Method

Figure 11 shows the theoretical model known as the source-source-sink model with its associated pressure distribution on the tunnels walls. The method discriminates between a wake line source at position X_2 with span b_w giving an asymmetric wake with a downstream asymptote and a line source (located at X_3) and sink at a distance C_s from each other, both with span b_s, producing the symmetric solid/bubble blockage pressure footprint. The locations are non-dimensionalized with the width of the test section B.

For this method the initial nonlinear system with seven variables was simplified by taking all three source spans equal, by estimating them from the model geometry and by assuming that the wake source is placed midway between the solid blockage source and sink. Figure 12, taken from Agardograph 336 (Ewald 1998) but slightly modified, presents the wall velocity distribution of the two distinct blockage contributions.

The curves for solid blockage and wake blockage are indicated with index sb and wb, respectively. A_{ts} is the test section area. Also indicated is the half-width at half-height location of the symmetric solid-blockage curve, $\Delta x/B$.

To compute the position and strength of the sources and sink, the required iteration procedure starts with determining the wake source strength Q_w from the

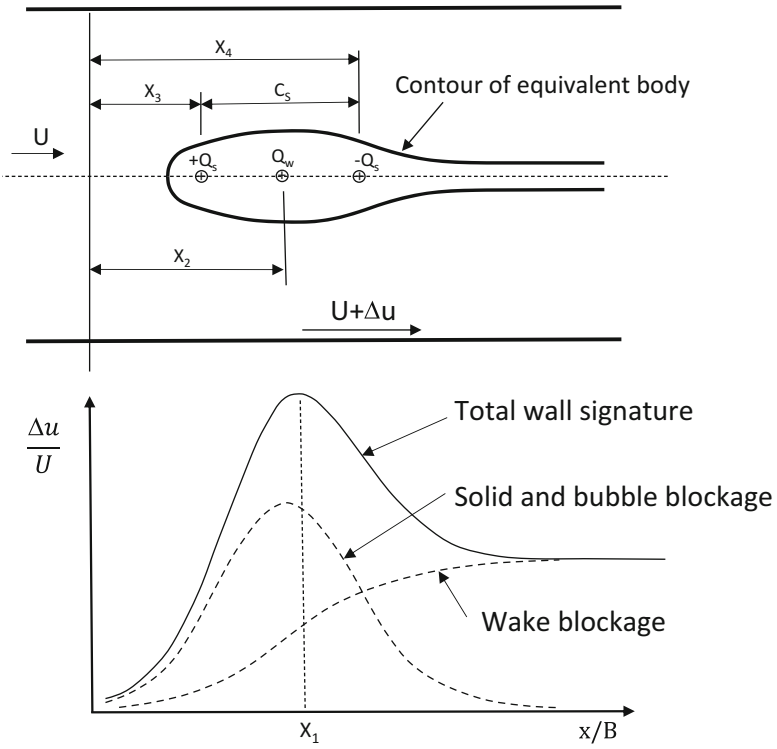

Fig. 11 The theoretical model of the source-source-sink method (Hackett and Wilsden 1975) with the associated wake and solid/bubble blockage super velocity components along the wall

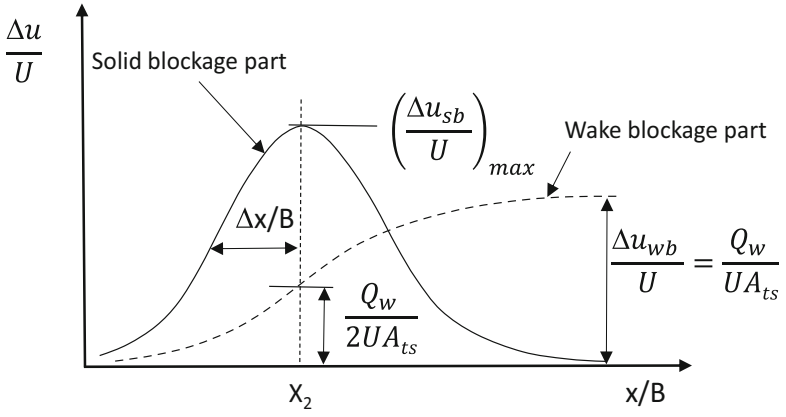

Fig. 12 The symmetrical and asymmetrical components of the wall pressure signature

asymptote $\Delta u_{wb}/U$, which is equal to Q_w/UA_{ts}, where A_{ts} is the width B times the height h of the test section. The next step is to estimate the position X_2 of the wake source, which may initially be taken equal to the model position. Then the wall signature of this wake source alone is calculated and subtracted from the measured velocity distribution to receive a first estimate of the symmetric solid blockage signature. If the location of the top of this distribution coincides with the value for X_2 the fitting is complete. If not, the calculation is repeated for a new value of X_2, until convergence is reached with a predefined accuracy. Next, the half-width at half-height $\Delta x/B$ and the dimensionless peak velocity $\Delta u_{wb}/U$ of the solid blockage distribution are determined. The remaining components, such as the source-sink strength and spacing, can now be computed using graphs or lookup tables. With all the ingredients known the method of images can be used to determine the interference velocity at the model location. Further details of the method can be found in Ewald (1998) and a computer code is presented in Hackett et al. (1979).

Allmaras (1986) presents a method for two-dimensional testing with a few alterations in the original, essentially three-dimensional, theoretical model among which an additional negative wake source of equal strength far downstream to satisfy mass conservation. In addition, the wake blockage velocity distribution is approximated by a hyperbolic tangent function. Allmaras' formulation results in a wake source strength deviating from Hackett's by a factor of 2 for a given velocity distribution. Computations with data from a wing test having blockage corrections of about 10% of the measured drag were in good agreement with the results obtained using simpler methods. In the appendices Allmaras gives a description of the necessary steps and look-up tables to compute the parameters for his theoretical model.

The Matrix Version of the Wall Signature Method

The matrix version of the pressure signature method uses multiple sources and vortex arrays, it is faster, it can handle more complex model geometries, and it performs better when dealing with more complicated lift-blockage couplings than the method described above. Interference effects are resolved by setting up influence matrices for the effects at the tunnel walls of the singularities that represent the model. In Hackett and Wilsden (1975) and Hackett et al. (1979) the method is described and a computer program is provided.

The matrix method was used by Wang et al to correct the measurements presented in Fig. 9a. They used 7 sources and 11 vortices to complete the theoretical model. The pressure distribution was captured by 135 pressure taps along the ceiling and floor of the 8 m long test section. The result is depicted in Fig. 13. The corrected drag curves for c/h values of 0.167 and 0.217 are in good agreement, but the curve for c/h= 0.267 seems to be over corrected. This may be due to the large scatter for this configuration which might also have been reflected in the wall pressure distribution. This will have made the construction of the theoretical model and the

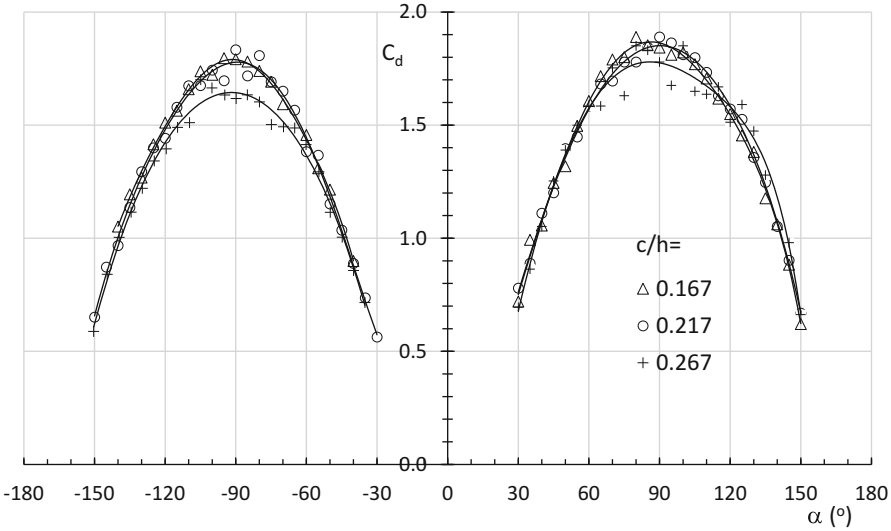

Fig. 13 The drag coefficients from Fig. 9a corrected with the matrix version of the wall pressure method (Wang et al. 2015)

associated fitting to the wall super velocity more difficult, despite the careful least squares curve fitting that is generally required. In this respect Maskell's method in Fig. 9b gives better results. Figure 14 presents the differences between the matrix version and Maskell's correction of the drag curve for c/h= 0.217. Here, the matrix version of the wall signature analysis produces slightly larger corrections compared to Maskell's method using $\theta = 0.96$, with a difference in $C_{d,\,max}$ in the order of 3.5%. The corrected curves coincide for $\theta = 1.04$.

Data Accuracy

A relatively smooth wall pressure distribution is of paramount importance for a good computation of the various model components. If the test section is too short, the wake blockage asymptote at high blockage ratio's may not be found with sufficient accuracy, which will have its repercussions on the rest of the calculations. If the pressure distribution is too scattered around the peak of the symmetrical velocity perturbation distribution, the solid blockage correction might not be accurately determined, even with additional least squares curve-fitting. Although a number of methods exist to cure measured pressure distribution deficiencies, the first aim should be to produce a smooth curve, which requires a pressure orifice distribution with enough resolution to capture the upstream and downstream asymptotes and the peak of the solid blockage velocity distribution. As the magnitude of the wall pressures is generally lower than the model surface pressures, sensors with

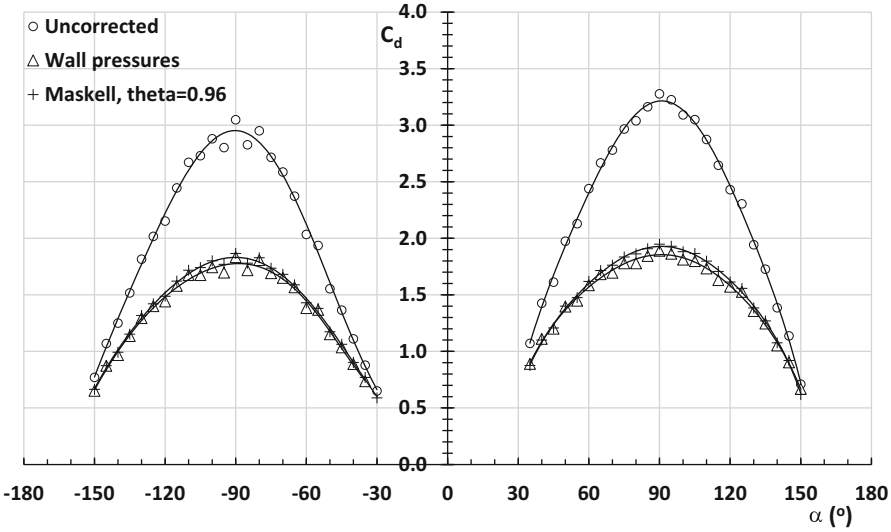

Fig. 14 The measurements from Wang et al. (2015) corrected with the matrix version of the wall pressure method and with Maskell's method using $\theta = 0.96$, c//h=0.217

a sufficiently low pressure range need to be selected. Furthermore, when capturing the flow dynamics is not an objective, long sampling times will greatly improve the curve quality.

Summary

Measurements on two-dimensional models in closed-wall test sections need to be corrected for the presence of the walls. Computation of the interference effects with the classical correction equations for attached flow give good agreement for chord-to-test section height ratios c/h of at least 0.36 in the range of angles of attack between -20 and 20 degrees. In the deep-stall region, when the boundary layer separates from the leading edge, Maskell's method with a blockage parameter $\theta = 0.96$ seems to give good results up to c/h values of 0.267, while the matrix version at this chord-to-height ratio seems to over-correct, also compared to the matrix-version results at the lower c/h values. At c/h= 0.217, the matrix version produces a 3.5% lower maximum drag coefficient compared to the result with Maskell's method, but the difference vanishes when $\theta = 1.04$ is used.

References

Allen HJ, Vincenti WG (1947) Wall interference in a two-dimensional wind tunnel, with consideration of the effect of compressibility. NACA Report no. 782

Allmaras SR (1986) On blockage corrections for two-dimensional wind tunnel tests using the wall-pressure signature method. NASA Technical Memorandum 86759

Ewald BFR (Ed) (1998) Wind tunnel wall corrections. AGARDograph 336

Fage A, Johansen FC (1927) On the flow of air behind an inclined flat plate of infinite span. British ARC R&M, No. 1104

Garner HC, Rogers EWE, Acum WEA, Maskell EC (1966) Subsonic wind tunnel wall corrections. AGARDograph 109

Glauert H (1933) Wind tunnel interference on wings, bodies and airscrews. British ARC R&M, No. 1566

Hackett JE (1996) Tunnel-induced gradients and their effect on drag. AIAA 34th Aerospace Sciences Meeting, Reno NV, Jan. 1996, paper 96-0562. AIAA Transactions, Vol. 34, No. 12

Hackett JE, Wilsden DJ (1975) Determination of low speed wake blockage corrections via tunnel wall static pressure measurements. Proceedings of the AGARD Symposium on Wind Tunnel Design and Testing Techniques, AGARD CP174, Paper 22

Hackett JE, Wilsden DJ, Lilley DE (1979) Estimation of tunnel blockage from wall pressure signatures: a review and data correlation. NASA CR-152, 241

Lock CNH (1929) The interference of a wind tunnel on a symmetric body, British ARC R&M, No. 1275

Maskell EC (1963) A theory of the blockage effects on bluff bodies and stalled wings in a closed wind tunnel. British ARC R&M, No. 3400

Wang L, Jiao Y, Gao Y (2015) Airfoil wind tunnel correction for angles of attack from -180°to 180°. Wind Energy 18:1487–1500